

Examination of type II origin with SOHO/LASCO observations

K.-S. Cho,¹ Y.-J. Moon,¹ M. Dryer,^{2,3} A. Shanmugaraju,⁴ C. D. Fry,⁵ Y.-H. Kim,¹ S.-C. Bong,¹ and Y.-D. Park^{1,6}

Received 13 August 2004; revised 18 July 2005; accepted 7 August 2005; published 3 December 2005.

[1] We examine a possibility that metric type II solar radio bursts are all caused by coronal mass ejection (CME) generated shocks. For this we consider 129 type II flare events from February 1997 to October 2000 and examine their associations with SOHO/LASCO CMEs according to their temporal and spatial closeness using SOHO/EIT and GOES data. We then carefully inspected 26 CME-less events to examine if there are CME-related features in LASCO and EIT images. In addition we examined 28 limb type II CME events to compare the kinematics of coronal shocks with those of the CME fronts. Under the assumption that the observed type IIIs are all generated by CME-related shocks, we determine the formation heights of the CME-associated type IIIs using LASCO CME speeds and type II onset times. From these studies, we have found (1) a large fraction (81%) of the type II bursts have temporal and spatial association with CMEs, and the association increases as their source position approaches to the limb; (2) most of the events without the association are related with weak flares and/or disk events; (3) most of the events are super-Alfvénic with a mean speed of 900 km s^{-1} ; (4) the front heights of all CMEs except for a few events are in the range of 1 to 3 solar radii, which are consistent with the type II formation heights; (4) the onset time difference (CME-type II) of all events are within about ± 1 hour, mostly -30 min to 10 min; (5) the CME speeds have a possible correlation ($r=0.6$) with coronal shock speeds, when two outliers are excluded. Considering a possibility that some outliers could result from some effects such as the coronal shock generation at CME flanks and CME accelerations, our results show that most of the type II bursts can be explained by the CME origin.

Citation: Cho, K.-S., Y.-J. Moon, M. Dryer, A. Shanmugaraju, C. D. Fry, Y.-H. Kim, S.-C. Bong, and Y.-D. Park (2005), Examination of type II origin with SOHO/LASCO observations, *J. Geophys. Res.*, *110*, A12101, doi:10.1029/2004JA010744.

1. Introduction

[2] Coronal type II radio bursts appear to be emission stripes slowly drifting from high to low frequencies in the dynamic spectrum. Although it is well known that the drifting stripes are the signature of coronal shock waves associated with flares and/or coronal mass ejections (CMEs), the physical relationship among metric type II bursts, flares, and CMEs is not well understood (for review, *Gopalswamy* [2000]). Actually, there has been the controversy about CME-flare-coronal type II burst association and relative timing [*Gopalswamy et al.*, 1998; *Cliver et al.*, 1999; *Cliver*, 1999; *Gopalswamy et al.*, 1999; *Leblanc et al.*, 2001]. This controversy is also related to a long-

standing critical issue on the relationship between CMEs and flares and their geoeffectiveness [*Gosling*, 1993; *Svestka*, 1995; *Gosling and Hundhausen*, 1995; *Sakai and de Jager*, 1996]. From the type II burst samples during solar minimum, *Gopalswamy et al.* [1998] proposed that type II bursts are produced by flares, and the fast CME-type II relation is to be understood as a proxy to the CME-flare relationship because the type II originating in the flare appears to be associated with the CME [see also *Dryer*, 1996]. Intimate onset time associations between flares and type II bursts have been reported by several authors [e.g., *Harvey et al.*, 1974; *Vrsnak et al.*, 1995; *Cho et al.*, 2003]. However, it is not resolved why the vast majority of flares are not associated with type II bursts. For this objective, special conditions were suggested in favor of a flare origin for type II bursts: (1) unusual low Alfvén speed in the flaring region [*Kahler et al.*, 1984]; and (2) short-lived flare sprays [*Gopalswamy et al.*, 1998]. On the other hand, it has been suggested that a CME is a special condition for generating type II bursts [cf. *Sawyer*, 1985; *Webb and Howard*, 1994; *Cliver et al.*, 1999]. In particular, *Cliver et al.* [1999] insisted that a Moreton wave in the chromosphere, a type II burst and EIT wave in the low corona are driven by fast CMEs. Their main arguments are (1) type IIIs

¹Korea Astronomy and Space Science Institute, Daejeon, Korea.

²NOAA Space Environment Center, Boulder, Colorado, USA.

³Also at Exploration Physics International, Inc., Huntsville, Alabama, USA.

⁴Department of Physics, Arul Anandar College, Krumathur, India.

⁵Exploration Physics International, Inc., Huntsville, Alabama, USA.

⁶Also at Big Bear Solar Observatory, New Jersey Institute of Technology, Big Bear, California, USA.

are highly associated with fast CMEs; (2) type II speeds and the speeds of CMEs associated with type II were consistent within the observed range of speeds; and (3) approximately two-thirds of fast CMEs are accompanied by type II bursts. However, they admitted that comparison of CME speeds and type II speeds for individual events have produced discordant results [Gergely, 1984; Gopalswamy and Kundu, 1995]. As evidence for supporting the suggestion that CMEs are a special condition for type II bursts, they proposed that the association rate of limb type II events with CMEs is higher than that of disk events based on SMM, GOES X-ray data, and Solwind Coronagraph data. In addition, there have been several reports [Gopalswamy and Kundu, 1992, 1993; Pick et al., 1998; Willson et al., 1998; Bastian et al., 2001] that the meter-wavelength radio signatures observed by radioheliographs (e.g., Very Large Array, Clark Lake instrument, Nancay Radioheliograph) were temporally and spatially associated with the CMEs detected by coronagraphs.

[3] Recently, several investigations [e.g., Klassen and Aurass, 2002; Lara et al., 2003; Shanmugaraju et al., 2003c] were made to study the association of type IIs with flares and/or CMEs based on the observations of the SOHO/LASCO (Large Angle Spectrographic Coronagraph). Using 63 metric type II radio bursts together with SOHO/LASCO and GOES X-ray data, Klassen and Aurass [2002] suggested that type II radio burst excitation may be either due to flare related blast wave shocks, shocks driven by the CME leading edge, or the internal parts or the flanks of the CME. Lara et al. [2003] found that the CMEs associated with type II bursts are more energetic (wider and faster) than regular CMEs. In addition to this fact, Shanmugaraju et al. [2003c] showed that the parameters such as flare strength and duration are also important for type II generation. Keeping in mind that faster CMEs are associated with flares with larger importance [e.g., Moon et al., 2002], such statistical analysis cannot provide a definite answer concerning the origin of type II bursts [e.g., Gopalswamy et al., 1998; Shanmugaraju et al., 2003c].

[4] In this paper we address the question: is a CME a special condition for type II solar radio bursts? To examine a possibility that all type IIs are generated by only CME related shocks as Cliver et al. [1999] argued, we consider 129 type II-flare events and their associations with SOHO/LASCO CMEs. If we assume that the type II radio bursts are all generated by CME-related shocks, then it would be very natural to expect that the CMEs are located in the type II formation heights at the initial time of the burst. The CME speeds at the formation heights are also expected to be similar to those of coronal shocks, estimated from the drift rates of the bursts and a coronal density model, if they are the origin of the type II bursts. For the selected limb type IIs, we determine their extrapolated CME height (expected formation height of the type II bursts) at the initial time of the burst by using the first appearance time, speed, and height of CME from the online SOHO/LASCO CME catalog. In addition, we present the kinematic data of three type II-associated CMEs with LASCO C1 and Mauna Loa Solar Observatory (MLSO) Mk IV observations which enable us to obtain their formation heights without any extrapolation of CME speeds.

[5] In section 2 we explain our event selection and data analysis. We present a longitudinal distribution of type II

associated CMEs, type II formation height, and onset time and speed comparison between CME and type II in section 3. A brief summary and conclusion are delivered in section 4.

2. Data and Analysis

2.1. Data

[6] We used the 173 type II bursts and the associated flare information listed in Table 1 of Fry et al. [2003], who studied the forecast of the arrival time of interplanetary shocks at the Earth during the rise of the solar maximum year: from February 1997 to October 2000. The properties of the observed bursts and the estimated coronal shock speeds were provided from the U.S. Air Force Solar Telescope Network (now Solar Radio Spectrograph) observatories, the Culgoora Solar Observatory, Australia, and IZIMIRAN (Institute of Terrestrial Magnetism, Ionosphere and Radiowave Propagation) Solar Radio Laboratory, Russia. The shock speeds were determined by real-time decisions in many cases, sometimes an average for multiple site observations. Type II bursts are thought to be generated by Langmuir turbulence due to accelerated electrons at the shock [see, e.g., Kruger, 1979]. The coronal shock speeds were estimated from a coronal density model and drift rates of the type II bursts deduced from the frequency-time history in the dynamic spectrum. The adopted electron density model in most of the observatories is the one-fold Newkirk model [Newkirk, 1961]. In most cases, optical flare location and importance were available in Table 1 of Fry et al. [2003]. The solar surface locations of the associated flares were independently taken from National Geographical Data Center (NGDC) (ftp://ftp.ngdc.noaa.gov/STP/SOLAR_DATA/FLARES) and confirmed from the brightening in EIT images.

[7] To obtain the information of CME events which may be related with type II bursts, we have used the height-time data of the CMEs from the online SOHO/LASCO CME catalog (http://cdaw.gsfc.nasa.gov/CME_list/). Initial CME kinematics are estimated and compiled in this catalog from LASCO C2 and C3 images obtained during the same period of the type II events. The LASCO instrument is an externally occulted white light coronagraph that observes Thomson scattered visible light through a broadband filter. The LASCO has some advantages over previous coronagraphs [Brueckner et al., 1995]. First, LASCO has much improved instrumental capabilities characterized by very low stray-light, low noise levels, and large dynamic range. Second, it provides high-quality difference images between event images and preevent images since SOHO is located at the L-1 orbit with a very stable movement in its halo orbit around the Sun-Earth line. Third, it has a very wide field of view. These advantages provide the factor of two or more higher CME observing rate than the rate obtained from coronagraph observations for the previous solar minimum [Howard et al., 1997]. The C2 instrument covers the range of 2.0–6.0 R_{\odot} with a resolution of about 23'' and a pixel size of 11.9''. The C3 instrument images 3.7–32 R_{\odot} [Brueckner et al., 1995] with a resolution of about 113'' and a pixel size of 56''. SOHOEIT provides spectro-heliograms of the corona and transit region on the solar disk and up to 1.5 R_{\odot} above the solar limb. It allows diagnostics of solar plasma at center temperatures in the range of 6×10^4 to $3 \times$

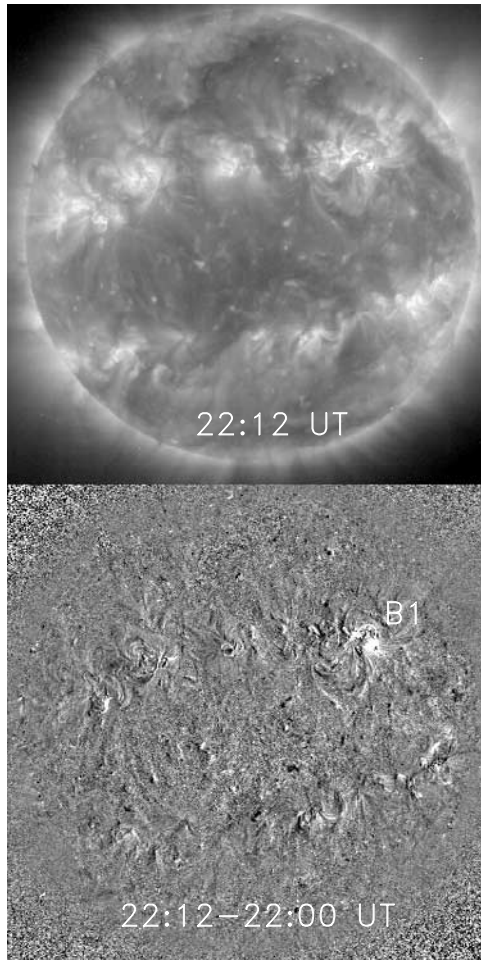


Figure 1. An extreme-ultraviolet imaging telescope (EIT) image (top) at 2212 UT in 6 November 1998 and its running difference image (bottom) of the coronal mass ejection (CME)-less type II event. B1 denotes a small EIT brightening associated with a SF optical flare.

10^6 K [Delaboudiniere *et al.*, 1995]. The time cadence of the EIT images used in this study is a few tens of minutes and their pixel resolution is about $2.6''$. The LASCO and EIT images as well as their running difference images are used for determining the association between the CMEs and the flares that are related to type IIs.

2.2. Event Selection

[8] Our data selection procedure is as follows. First, we have examined all 173 type II burst-flare events compiled by Fry *et al.* [2003] and the SOHO/LASCO images to inspect if the bursts have temporal closeness with CMEs. Unfortunately, 44 type II bursts occurred during LASCO data gaps, thereby reducing the number of our data set from 173 to 129 events. Second, we identified 103 CMEs whose LASCO C2/C3 first appearance times are within a threshold window (90 min) from the type II starting time. The longitudinal distribution of these CMEs (103 events) is examined and then compared with the distribution of type IIs (26 events) without CMEs in the following section. We have carefully examined the 26 CME-less type II events to examine if there are CME-related features such as a bow

wave [Gopalswamy *et al.*, 2001] using EIT images and their running difference images. In most cases, we cannot see any bow wave features but small EIT brightenings related to corresponding flares. Figure 1 presents a set of EIT and its running difference image showing a small EIT brightening (denoted B1) related to the 6 November 1998 event, which is one of the CME-less events. Table 1 summarizes the EUV and CME features seen from SOHO/EIT and SOHO/LASCO C2 data near the time of the CME-less type II burst. The first six columns give the information of type II bursts and their associated flares. There are 11 CMEs that are not likely to be associated with type IIs or to have some ambiguities; they are denoted as east, bipolar, backside, and pre-CMEs in Table 1. We noted that among the 15 events marked as “No CME detected” in Table 1, 13 events are disk events and most of them are associated with weak flares. Such weak disk events may not be detected by LASCO due to the visibility problem as suggested by Cliver *et al.* [1999] and Gopalswamy *et al.* [2001]. For the remaining two limb events (27 July 2000 and 1 August 2000), we can see a weak LASCO enhancement and EUV dimming above the eruption region.

[9] For the comparison of the characteristics of type II shocks and CMEs, we selected 28 limb events whose solar surface longitudinal positions are greater than 60 degrees. Their associated CMEs are well detected in LASCO C2/C3 instrument. Table 2 summarizes the details of these 28 type II bursts. The first four columns give the information of type II events and their associated flare such as type II start date and time, flare location, and flare start time. The next four columns represent the first CME appearance time and height (in solar radii) in the C2 or C3 images, the position angle, and the initial speed estimated from the first two height-time data in the LASCO field of view. The type II burst information is given in the last three columns as follows: the start frequency of the bursts; the shock speed estimated by employing one-fold Newkirk model [Newkirk, 1961]; the difference between the first C2/C3 appearance time of the CME and the starting time of the type II bursts.

3. Results and Discussion

[10] To illustrate the close temporal relationship among type II burst, flare, and CME, we present their time sequences and speeds for a well observed event on 11 June 1998 in Figure 2. As seen in the figure, the type II burst occurred in the eruptive phase of the flare, and the CME speed at this time is comparable to the typical coronal Alfvén speed. Thus we can expect either possibility; that is, the type II shocks can be generated by either the CMEs or the flares. In this section we will examine their several characteristics to address our main question: Can all type II bursts be generated by CME related shocks?

3.1. Longitudinal Distribution of the CMEs

[11] To examine if type II bursts linked to a flaring region within 30° of the solar limb are associated with fast ($>400 \text{ km s}^{-1}$) CMEs [Cliver *et al.*, 1999], we have examined the longitudinal distribution of the selected 129 type II bursts out of 173 type IIs compiled by Fry *et al.* [2003]. Out of 129 events, 105 events including two identified CMEs in Table 1 have their associated CMEs, and the remaining

Table 1. Information of CME-less Type II Bursts and the Associated Flares

Date	Type II Start	V_s^a	Pos (deg)	Flare Start	Flare Strength	Description EIT and CME features
97/02/07	02:30	600	S49W02	-	-	Pre-CME at 00:30 UT in LASCO C2
98/11/06	22:11	1138	N15W37	22:05	SF	No CME detected, EIT brightening
99/02/20	04:16	700	S21W63	04:00	SF	East CME at 05:30 UT in LASCO C2
99/02/20	15:27	800	S17W21	15:11	SF	Bipolar CME at 15:54 UT in LASCO C2
99/05/08	14:52	800	N23W75	14:22	SF	Pre-CME at 14:50 UT in LASCO C2
99/05/26	02:35	650	N27E39	02:25	SF	No CME detected, EIT brightening
99/07/01	01:48	600	S15W16	01:41	SF	No CME detected, weak EIT brightening
99/08/02	05:40	500	S28W28	05:28	SF	No CME detected, weak EIT brightening
99/08/02	09:59	600	N26W01	09:42	SF	No CME detected, EIT brightening
99/08/17	14:42	600	S17W81	14:28	SF	Pre-CME at 13:31 UT, EIT eruption
99/08/21	16:52	500	S25E56	16:30	1B	Pre-CME at 16:50 UT, EIT eruption
99/10/27	13:29	500	S16W87	13:24	SF	East CME at 13:50 UT, EIT eruption
99/12/06	07:18	500	N10E43	07:00	2N	No CME detected, EIT brightening
00/02/17	20:24	550	S29E07	20:17	2N	Pre-CME at 20:06 UT, EIT eruption
00/03/21	14:21	1200	N31W36	14:12	SF	Backside CMEs appeared at 14:30 UT
00/04/12	06:32	500	S19W28	06:22	SN	No CME detected, weak EIT brightening
00/06/14	13:49	928	N23W32	13:44	1F	Pre-CME at 13:26 UT, weak EIT brightening
00/06/20	19:32	980	N19W28	19:21	1N	No CME detected, No EIT data
00/06/21	08:12	700	N19W37	07:56	1N	No CME detected, EIT brightening
00/07/07	03:18	700	N21W37	-	SF	No CME detected, EIT brightening
00/07/07	11:14	800	N23W41	10:56	SN	No CME detected, No EIT data
00/07/21	14:40	580	N10E12	14:30	SF	No CME detected, EIT brightening
00/07/27	04:11	850	N10W72	04:06	SB	Weak CME, EIT dimming
00/08/01	03:47	750	N15E90	03:37	SF	Weak CME, weak EIT dimming
00/08/28	17:13	911	S17E24	16:56	1N	No CME detected, EIT brightening
00/09/12	12:07	1030	S17W09	11:31	2N	Pre-CME at 11:54 UT, EIT brightening

^aIndicates the coronal shock speed (km s^{-1}) derived from type II radio burst using one-fold Newkirk model.

events (24) do not show clear associations. Figure 3 shows the longitudinal distribution of the type II radio bursts with CMEs (105) and without CMEs (24). Solid histogram indicates the distribution of all type II radio

bursts (129) under consideration, and the dashed histogram shows the distribution of type II bursts associated with CMEs. As seen in the figure, the numbers of all type IIs as well as the type IIs associated with CMEs

Table 2. Characteristics of Type II Burst, Flare, and CME for the Selected Limb Events

Date	Type II Start	LOC (deg)	Flare Start	CME Time	CME C2/C3	PA (deg)	V_i^a	f_s^b	V_s^c	ΔT_{CI} (min)
97/11/27	13:17	N20E60	12:59	13:57	3.42	98	515	85	A700	40
98/12/18	17:27	N21E69	17:13	18:22	9.84	36	1718	50	S1200	55
99/03/08	06:38	S22E76	06:30	06:54	2.30	115	765	F200	C700	16
99/04/03	23:06	N18E62	22:56	23:47	5.51	74	1040	F90	H500	41
99/04/04	04:16	S10E90	-	05:54	6.64	65	1311	F50	P600	98
99/05/29	03:11	S20E80	03:04	03:26	2.65	81	777	F90	P600	15
99/06/11	11:16	N38E90	11:07	11:26	2.74	35	1454	85	A900	10
99/07/16	15:55	N43W71	15:42	16:30	4.72	301	821	F50	S800	35
99/07/25	13:21	N38W81	13:08	13:31	3.10	284	1454	80	S1000	10
99/08/04	05:52	S16W64	05:45	06:26	2.31	262	386	F110	V462	34
99/08/20	18:39	S23E66	18:25	18:50	3.29	84	667	50	P400	11
99/08/20	23:17	S25E64	23:03	23:26	4.03	111	1218	F50	P700	9
99/09/21	03:12	N24W88	03:00	03:54	3.18	298	1330	F90	C900	42
99/10/26	21:30	S13W74	21:09	21:50	2.68	256	450	F70	C400	20
00/02/18	09:20	S16W78	09:21	09:54	4.15	286	1102	F75	V1400	34
00/03/03	02:12	S15W60	02:08	02:30	2.70	233	874	F90	A550	18
00/03/18	21:05	S16W64	20:47	21:30	2.45	300	483	F70	P730	25
00/04/04	15:25	N16W66	15:12	16:43	12.44	265	1107	F65	A2000	78
00/04/28	18:49	N19W60	18:43	19:31	3.45	271	296	80	P500	42
00/06/15	19:46	N20W65	19:38	20:06	4.36	298	1372	84	H996	20
00/06/18	01:58	N23W85	01:52	02:20	2.87	307	370	F65	P660	22
00/06/23	14:20	N26W72	14:18	14:54	4.71	282	1005	84	H960	34
00/06/28	18:58	N20W90	18:48	19:32	6.43	270	1214	80	H536	34
00/07/12	20:14	N17W65	20:00	20:30	3.07	281	828	80	S950	16
00/08/25	07:50	S17E69	07:31	08:30	2.72	83	275	83	V767	40
00/08/25	14:35	S15E67	14:21	14:54	2.67	49	580	80	S1600	19
00/09/01	18:27	N10W60	18:05	18:54	2.63	244	469	75	S500	27
00/09/09	08:40	N07W67	08:28	08:57	3.22	271	969	180	A1095	17

^aIndicates the initial speed (km s^{-1}) of CME in the LASCO field of view.

^bIndicates the start frequency in MHz of type II radio burst. “F” indicates the fundamental frequency. Otherwise, the emission mode is unavailable.

^cIndicates the coronal shock speed (km s^{-1}). “A” indicates an average speed for multiple site observations, “S” for Sagamore Hill (Massachusetts), “P” for Palehua (Hawaii), “H” for Holloman (New Mexico), and “V” for San Vito (Italy).

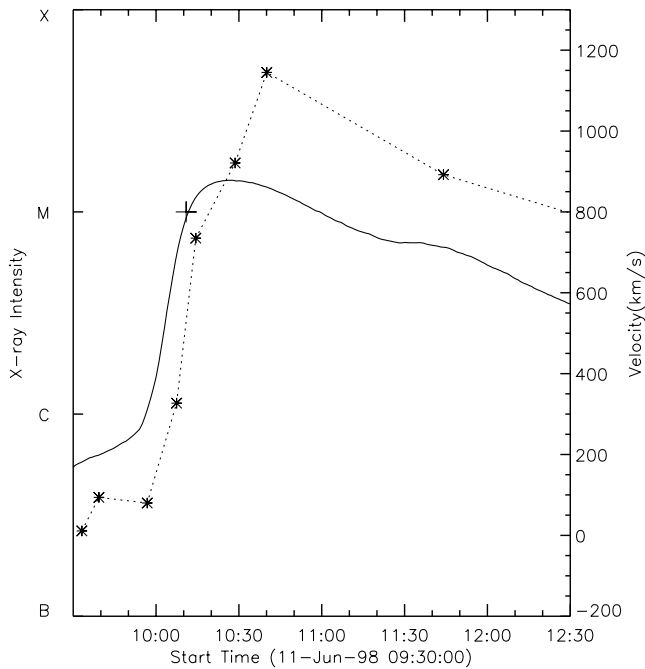


Figure 2. Velocity-time data of the type II burst (plus symbol) and the CME (asterisk symbol from LASCO C1, C2, and C3) observed on 11 June 1998 together with GOES X-ray flux (solid line).

decrease with the distance from the central meridian. However, the association of type II with CMEs increases as the source position approaches the solar limb, which is consistent with *Cliver et al.*'s [1999] argument. The fraction of type II bursts associated with CMEs in each bin are 75% (39/52) for $0^\circ \leq L < 30^\circ$, 83% (35/42) for $30^\circ \leq L < 60^\circ$, and 89% (31/35) for $60^\circ \leq L \leq 90^\circ$. On an average, about 81% (105/129) of the events have temporal and spatial association with CMEs.

3.2. Type II Formation Height

[12] If a type II burst was generated by the shock formed at the CME leading edge, we can simply assume that the CME front at the starting time of the type II burst would be located at the type II burst emitting region, and its speed should be greater than the local Alfvén speed. Under this assumption, we consider the 28 limb CMEs whose solar surface longitudinal position is greater than 60° to minimize the projection effects; that is, real heights above the solar surface of disk events could be underestimated by the projection effect. We determined their extrapolated heights at the start times using the constant speed method. The height can be simply derived like $H(\text{type II}) = R_c - V_c T_{cv}$, where R_c is the first appearance position of CMEs in LASCO C2/C3 field of view, T_{cv} is the difference between the first appearance time of the CME and the start time of the type II burst, and V_c is the initial speed estimated from the first two height-time data in the LASCO field of view.

[13] The constant speed method (linear speed assumption) has been used by several researchers [e.g., *Harrison*, 1986; *Harrison*, 1995; *Moon et al.*, 2002; *Zhang et al.*, 2002; *Andrews*, 2003; *Cho et al.*, 2003] to estimate the CME onset times, since we have insufficient kinematic

information of CMEs at the time of type II radio bursts in many cases. We also take the same extrapolation method using the first two height-time data in the LASCO field of view. According to the recent works such as *Zhang et al.* [2001], *Neupert et al.* [2001], and *Shanmugaraju et al.* [2003b], the impulsive acceleration phases of the CMEs are coincident with the impulsive phases of GOES X-ray flares, and their accelerations nearly stop after the flare peak times. In the case of most of our samples, the event times of type IIs are just before the flare peak times or after. Most of the exceptional events are long duration events whose peak X-ray fluxes were sustained for a long time. According to *MacQueen and Fisher* [1983], the speeds of flare-associated CMEs are nearly constant at the coronal region from 1.4 to 2.4 solar radii (for details, see Figure 3 in their paper). These facts imply that the errors of the linear extrapolated heights at the time of type II radio bursts are less serious than in the case of CME onset time estimates.

[14] Figure 4 shows the CME initial speeds and their formation heights extrapolated using the constant speed method at the starting times of related type II bursts. Most of the events are located within the range of 1 to 3 solar radii. Following *Mann et al.* [1999], we adopt the local Alfvén speed determined by using the magnetic field distribution:

$$B(R) = 2.2 \times (R_\odot/R)^2 [G] \quad (1)$$

in the quiet Sun. Note that the shock speeds used in this study were taken from several observatories whose shock speeds were usually estimated using the number density model of one-fold Newkirk model:

$$N_e(R) = 4.2 \times 10^{4+4.32(R_\odot/R)} [\text{cm}^{-3}] \quad (2)$$

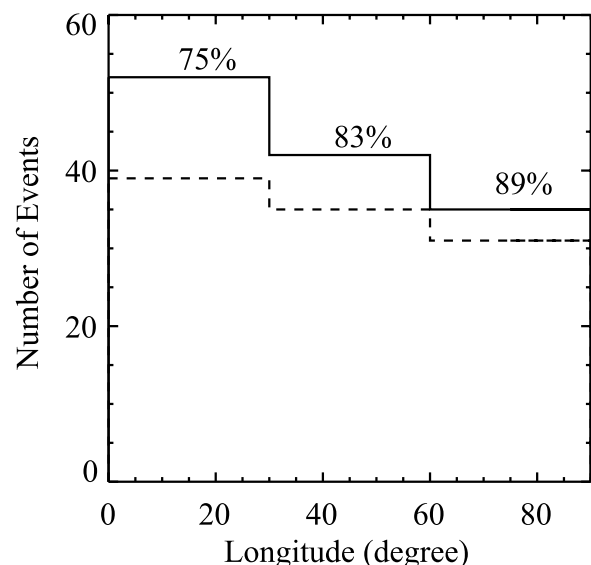


Figure 3. Histogram of the longitudinal distribution of type IIs with CMEs. Solid line: breakdown of 129 type II events (February 1997 to October 2000) after 44 SOHO/LASCO data gaps were deleted from a grand total of 173 type II events compiled by *Fry et al.* [2003]. Dashed line: total of 105 type II events associated with CMEs within 90 min window from the start time of type II burst.

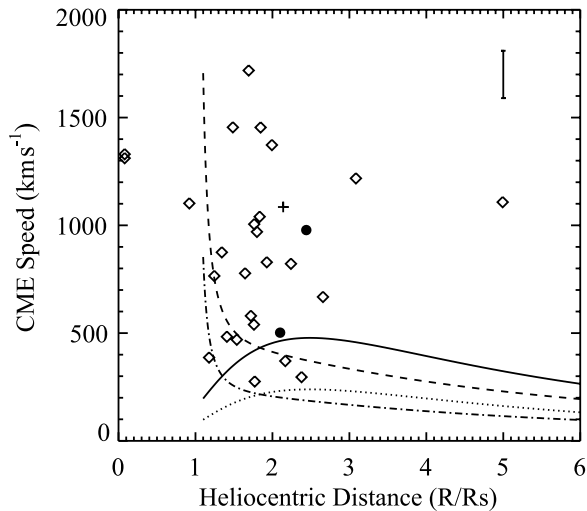


Figure 4. CME speed vs type II formation height extrapolated using the constant speed method. The original locations of two events near the heliocenter, which were estimated from the extrapolations, are $-4.4R_{\odot}$ and $-1.6R_{\odot}$, respectively. Speeds and heights of the CMEs measured with LASCO C1 and MLSO Mk IV observations are designated by cross and filled circle symbols, respectively. Alfvén speeds are computed using one-fold Newkirk density model (solid line) and four-fold Newkirk model (dotted line) for the quiet magnetic field model. The speeds are also estimated using one-fold Newkirk model (dashed line) and four-fold Newkirk model (dash dot line) for the active region magnetic field model. The error bar in right upper corner indicates the mean error (110 km s^{-1}) of extrapolation estimated from three events in Table 3.

[Newkirk, 1961]. To take into account both the density effect and magnetic field effect, we also consider local Alfvén speed profiles derived by using one-fold Newkirk model (dashed line) and four-fold Newkirk model (dash-dotted line) with the active region magnetic field model [Gopalswamy *et al.*, 2001] given by $B(R) = 0.5 \times (R/R_{\odot} - 1)^{-1.5} [G]$.

[15] Our approach is the first trial to examine the CME origin of type II bursts by comparing type II formation height and CME kinematics. One disadvantage of our approach is that the speeds of the CMEs at the time of type II formation are extrapolated from LASCO C2 data. To relieve this disadvantage, we analyzed three type II associated limb CMEs whose LASCO C1 and MLSO Mk IV data are available. Their detailed information is summarized in Table 3. Two events (26 October 1999 and 28 June 2000)

from MLSO in this table are also listed in Table 2. The first two columns list the date and start time of the type IIs. The next four columns give the times ($T_1 = \text{before}$, $T_2 = \text{after}$) and the heights of CMEs near the event times of type II bursts. The seventh and eighth columns show the height of the CME at the type II start time and its speed at that time, respectively. The used instrument (C1 or Mk IV) and the CME speed error, estimated by assuming an 8-pixel measurement uncertainty in each image of the instrument, are described in the last two columns.

[16] In Table 3 the first CME was observed by the LASCO C1 coronagraph near the start time of type II bursts. The height and speed of the CME at the time of type II burst was determined by using spline interpolation of the height-time data of the CME from the online catalogue of SOHO/LASCO C1 events (http://solar.scs.gmu.edu/research/cme_c1/), in which initial CME kinematic data is estimated from LASCO C1 images. The LASCO C1 observes the lower corona from 1.1 to $3 R_{\odot}$ with a resolution of about $11''$ and a pixel size of $5.6''$ [Brueckner *et al.*, 1995]. We roughly estimate the error of the constant speed method in estimating the formation height using the type-II associated CME with LASCO C1 observation. The estimated difference (extrapolated from C2–C1 observation) of the extrapolated height is found to be $-0.35 R_{\odot}$. The difference of the CME speed (C2–C1 speed) is 43 km s^{-1} . Unfortunately, the coronal shock speed of the event is not available. The last two events in Table 3 were observed by MLSO Mk IV coronagraph which covers from 1.08 to $2.85 R_{\odot}$ with a pixel size of $6.09''$ [Elmore *et al.*, 2003]. The first event is a CME that appeared around 2120 UT on 26 October 1999 near the west limb of the Mk IV coronagraph image. It had two large ascending loops and a third, smaller loop ascending among the other two. The second event is a faint CME observed in 1846 UT on 28 June 2000. It was accompanied by an eruptive prominence having a similar shape with that of the CME in the LASCO field of view. The estimated differences (extrapolated from C2–Mk IV observation) of the extrapolated heights are found to be $-0.2 R_{\odot}$ and $0.43 R_{\odot}$, respectively. The difference of the CME speeds between (C2–Mk IV speed) are -52 km s^{-1} and 236 km s^{-1} , respectively. Using the three events in Table 3, we roughly estimated the speed error (110 km s^{-1}) from extrapolation as a mean of the differences between LASCO C2 speed and low coronal speed. These three events are included in Figure 4 with different symbols.

[17] As seen in Figure 4, most of the events have speeds higher than the Alfvén speed with a mean speed of 900 km s^{-1} . The number of super Alfvénic events might be changed according to the coronal magnetic field and electron density models. If we consider the one-fold Newkirk density model

Table 3. Information of Type II Associated CMEs With LASCO C1 and MLSO Mk IV Observations

Date	Type II Start	CME T_1	$H(T_1) (R_{\odot})$	CME T_2	$H(T_2) (R_{\odot})$	$H_{II}^a (R_{\odot})$	$V_c^b (\text{km s}^{-1})$	Observation	Error ^c (km s^{-1})
98/06/11	10:10:54	10:07:27	1.85	10:11:24	2.19	2.14	1085	C1	207
99/10/26	21:30:00	21:27	1.97	21:30	2.1	2.1	502	Mk IV	34
00/06/28	18:58:00	18:55:31	2.19	18:58:29	2.44	2.44	978	Mk IV	35

^aIndicates the height of CME at the start time of type II radio bursts in the LASCO C1 and Mk IV fields of view.

^bIndicates the speed of CME at the time of type II radio bursts.

^cIndicates the CME speed error from the 8 pixel uncertainty of LASCO C1 and Mk IV measurements.

and the quiet magnetic field model, all the events except for three events are super-Alfvénic. If we consider the four-fold Newkirk density model and the quiet magnetic field model, as seen by the dotted curve in Figure 4, all three exceptional events become super Alfvénic. The front heights of all CMEs except for a few events are in the range of 1 to 3 solar radii, which are consistent with the type II formation heights. The exceptional events may be explained by considering the projection effect of CMEs (one event near 5 solar radii) and/or strong variation of CME kinematics (two events near the heliocenter) in the low corona [e.g., Zhang *et al.*, 2001; Neupert *et al.*, 2001; Gallagher *et al.*, 2003; Shanmugaraju *et al.*, 2003b].

3.3. Onset Time and Speed Comparison

[18] In this section we investigate the relationship between CMEs and type II bursts with respect to their onset time and the speed comparisons. For these comparisons, we used 28 events in Table 2. Considering the above-mentioned two CMEs (99/10/26 and 00/06/28), we used the CME information in Table 3, estimated by MLSO Mk IV observations, instead of the extrapolated onset times and speeds from LASCO C2/C3 observation.

[19] The comparison of the onset time difference between CMEs and type IIs is a simple way to give us some hints on the question: is a CME the driver of the type II burst? There have been several attempts to examine the association between type II bursts and CMEs based on the onset time difference [e.g., Robinson and Stewart, 1985; Lara *et al.*, 2003; Klassen and Aurass, 2002; Cho *et al.*, 2003; Shanmugaraju *et al.*, 2003a]. For most cases, the onset time of a CME was often extrapolated by assuming that the initial height of the CME is around $1.1 R_{\odot}$. In this study we extrapolated the onset time of a CME from the LASCO first appearance position to the height $1.3 R_{\odot}$ using the constant speed method; in this study the CME onset time is assumed when a CME is located at the height $1.3 R_{\odot}$, since the mean starting frequency (83 MHz) of our type II data corresponds to the height when we use the one-fold Newkirk density model. Thus the CME onset time can be estimated like $T_o = T_c - (R_c - 1.3R_{\odot})/V_c$, where R_c is the initial position of the CME, T_c is the first appearance time of CMEs, and V_c is the initial CME speed. We estimated their onset times for the selected limb events in Table 2. Figure 5 shows the histogram of the difference between the type II start time and the CME onset time for these 28 events. As shown in the figure, their onset time difference (CME–type II) approximately follows a normal distribution ranging from -50 min to $+50$ min, mostly -30 min to $+10$ min. Their mean difference is about -10 min. These results show a close temporal association between CMEs and type IIs at the shock formation height.

[20] The comparison between the CME speed inferred from white-light coronagraph images and the coronal shock speed estimated from the drift rate of type II radio emission is a way to study the association between CME dynamics and the shock dynamics. While Reiner *et al.* [2001] found no obvious correlation between shock speeds derived from type II bursts and the corresponding CME speeds, Shanmugaraju *et al.* [2003a] found a possible correlation between type II speed and CME speed in the case of double type IIs. Figure 6 shows the comparison of the

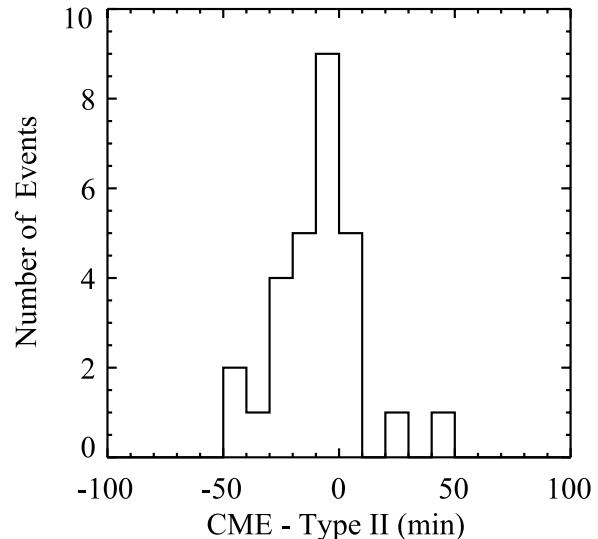


Figure 5. Histograms showing the onset time difference between CME and type II burst using 10 min bins.

CME speed at the starting time of type II burst and the shock speed estimated by using one-fold Newkirk model. As seen in the figure, a weak correlation ($r = 0.4$) was obtained between the CME speed and the shock speed. If two outliers in the top of the figure are excluded, the correlation becomes more evident ($r = 0.6$). This is similar to that ($r = 0.56$) of Shanmugaraju *et al.* [2003a]. The estimated shock speeds of these two events are unusually high, which may be overestimated due to a nonuniform density gradient in the ambient corona.

[21] In addition, some scattered points may be explained by the coronal shocks generated at the CME flank as follows. It is known that coronal shocks might be generated at the CME flanks, which were demonstrated by observations [Sheeley *et al.*, 2000] and numerical simulations [Dryer *et al.*, 1979; Vourlidas *et al.*, 2003]. In this case, the type II height is expected to be smaller than that of the CME front, and type II emission frequency becomes higher due to the large number density. However, the drift rate of the type II is lower than that from the CME front due to the low-density gradient. As a result, the type II speed generated at the flank is expected to be lower than that at the CME front (refer to equation (5) for details).

3.4. Density Effect

[22] In fact, the estimated type II speed depends on coronal density distribution. Thus one may think that the estimated speed difference between CME and type II speed can be explained by the change of coronal density. To examine such an effect, we estimate a distribution of the density multiplier for which the type II speed is consistent with the CME speed. Here, the density multiplier (α) is defined as follows:

$$N_e = \alpha \times \left(4.2 \times 10^{4+4.32(R_{\odot}/R)}\right) [\text{cm}^{-3}]. \quad (3)$$

The observed frequency of type II is generally assumed as being close to the local plasma frequency, i.e.,

$$f \sim f_p = 9000 \sqrt{N_e} [\text{Hz}]. \quad (4)$$

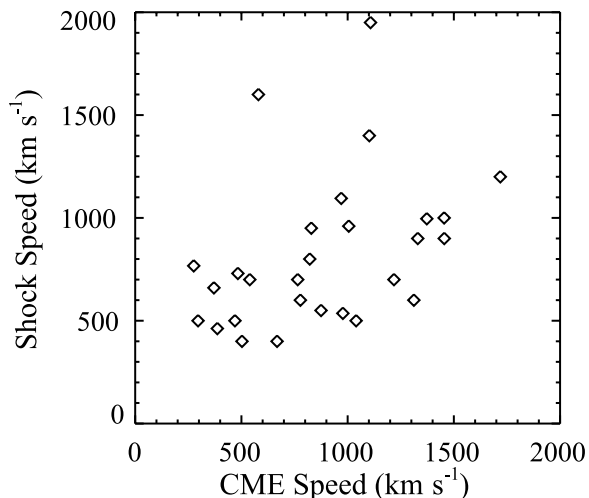


Figure 6. CME speed versus coronal shock speed. The CME speed is estimated from the first two height-time data in the LASCO field of view and the shock speed is derived from the one-fold Newkirk model and drift rate of type II burst deduced from the frequency-time data in the dynamic spectrum.

From equations (3) and (4), the type II shock speed has a relation with the square of inferred height (R) of type II emission as

$$V_s = \frac{-2 \times R^2}{\ln 10 \times 4.32 R_\odot} \frac{df}{dt} \frac{1}{f}, \quad (5)$$

where f is observing frequency and df/dt is a drift rate of type II burst. By rearranging equation (5), we can get the relation

$$\frac{R_\odot}{R} = \sqrt{\frac{-2}{\ln 10 \times 4.32} \times \frac{df}{dt} \frac{R_\odot}{f V_s}}. \quad (6)$$

[23] Figure 7 shows the density multipliers of all events using equations (3) and (6) together with the information in Table 2. It ranges from 0.006 to 10.9. In the figure the two dotted lines corresponds to the boundaries which takes into account two density enhancement and depletion regions: helmet streamers [Parenti *et al.*, 2000] and low-density regions [Guhathakurta and Fisher, 1998]. As shown in the figure, there is a large fraction (71%) of the events inside the boundaries, which can be explained by the density effects. For the events that are located within the boundaries, the difference between CME speed and type II speed can be explained by the coronal density effects under consideration. Most of the outliers outside the two boundaries correspond to highly scattered events shown in Figures 4 and 6. This fact implies that such events may be explained by the projection effect and/or CME strong accelerations, as already mentioned in previous subsections.

4. Summary and Conclusion

[24] In this paper we have examined a proposition that the origin of metric type II solar radio bursts are shocks that are

formed by coronal mass ejections (CMEs), as Cliver *et al.* [1999] argued. For this we examined the associations of 129 type II flare events with SOHO/LASCO CMEs according to their time closeness. We then inspected 26 CME-less events to identify if there are CME-related features in LASCO and EIT images. Under the assumption that the observed type IIs are all generated by CME generated shocks, we have determined the formation heights of the 28 limb CME-associated type IIs. In addition, we examined two type II associated CMEs with MLSO Mk IV coronagraph at the time of type II bursts to obtain their formation heights without any extrapolation of CME speeds.

[25] Our main results can be summarized as follows.

[26] 1. A large fraction (81%) of type II bursts seems to have temporal and spatial associations with CMEs. The association rate of type IIs with fast CMEs by SOHO/LASCO observations is higher than that (64%) by Solwind [Cliver *et al.*, 1999]. This result seems to be due to the improved sensitivity and extended field of view of LASCO instruments. The fraction of type II bursts associated with CMEs increases with the longitude of the source position. This result is consistent with Cliver *et al.* [1999] who argued that the association between type II bursts and CMEs would be high at the solar limb.

[27] 2. A careful inspection of LASCO CME images shows that most of the events without the association with CMEs are related with weak flare and/or disk events. Such weak disk events may not be detected by LASCO due to the visibility problem as suggested by Cliver *et al.* [1999] and Gopalswamy *et al.* [2001].

[28] 3. Most of the events are super Alfvénic with a mean speed of 900 km s^{-1} and the CME front heights of all events except a few events are in the range of 1 to $3 R_\odot$, which are consistent with the formation heights of type II bursts.

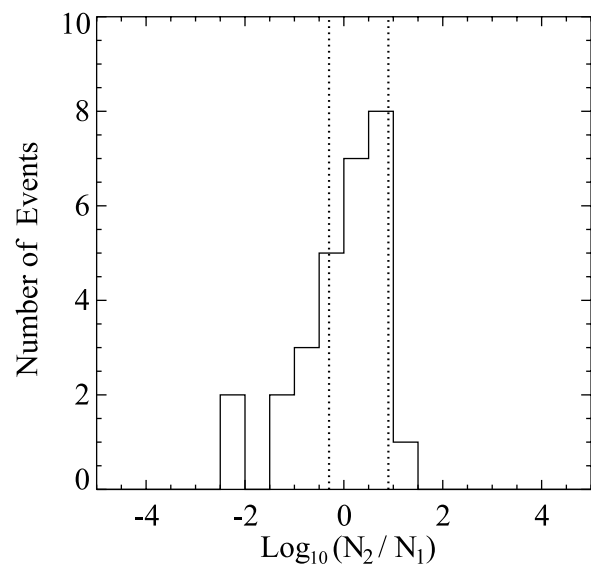


Figure 7. Distribution of the density multipliers for which the type II speed is consistent with the CME speed. Left vertical dotted line denotes the density of low-density region (0.5-fold Newkirk model) and right vertical line indicates that of coronal streamer (eight-fold Newkirk model).

[29] 4. The onset time comparison shows that all the CMEs occurred within about ± 1 hour, mostly -30 min to $+10$ min. This fact implies close temporal associations between type II bursts and CMEs.

[30] 5. When two outliers are excluded, a possible correlation ($r = 0.6$) is found between the CME speeds and coronal shock speeds. The estimated shock speeds of these two events are unusually high, which may be overestimated due to a nonuniform density gradient in the ambient corona.

[31] 6. By examining the distribution of the density multiplier for which the type II speed is consistent with the CME speed, we found that a significant fraction (70%) of type II bursts can be explained by the coronal density effects. Some exceptional events may be explained by the projection effect and/or strong accelerations of CMEs.

[32] Our results show that a significant fraction (70–80%) of the type II events can be explained by CME-generated shocks. It is also noted that the results are based on the fact that type II formation is temporally and spatially consistent with the CME front. If we include a possibility that type II bursts are generated at CME flanks [Sheeley *et al.*, 2000; Vourlidas *et al.*, 2003], the estimated fraction would be higher. Some outliers shown in Figures 4, 5, 6, and 7 may be explained by several effects such as the projection effect, coronal density anomaly, and strong CME accelerations. Thus these results seem to support Cliver *et al.* [1999], who argued that all type II bursts are generated by CMEs. However, we feel that further examinations by using low coronal observations without any extrapolation of CME kinematics are needed to draw a more definite conclusion on the CME origin of type II bursts.

[33] **Acknowledgments.** This work has been supported by the MOST grants (M1-0318-00-0059, M1-0336-00-0011, M1-0336-00-0013, and M1-0407-00-0001) of the Korean government. We would like to thank the referees' constructive comments YJM and YDP were supported by the Korea Research Foundation (KRF-2005-070-C00059) of the Korean government. MD and CDF were supported by NASA's Living With a Star (LSW) Targeted Research and Development Program via NASA grant NAG-12527. The CME catalog we have used is generated and maintained by the Center for Solar Physics and Space Weather, The Catholic University of America in cooperation with the Naval Research Laboratory and NASA.

[34] Lou-Chuang Lee thanks the reviewers for their assistance in reviewing this paper.

References

- Andrews, M. D. (2003), A search for CMEs associated with big flares, *Solar Phys.*, *218*, 216–279.
- Bastian, T. S., M. Pick, A. Kerdran, D. Maia, and A. Vourlidas (2001), The coronal mass ejection of 1998 April 20: Direct imaging at radio wavelengths, *Astrophys. J.*, *558*, L65–L69.
- Brueckner, G. E., *et al.* (1995), The Large Angle Spectroscopic Coronagraph (LASCO), *Solar Phys.*, *162*, 357–402.
- Cho, K.-S., K.-S. Kim, Y.-J. Moon, and M. Dryer (2003), Initial results of the Icho solar radio spectrograph, *Solar Phys.*, *212*, 151–163.
- Cliver, E. W. (1999), Comment on "Origin of coronal and interplanetary shocks: A new look with Wind spacecraft data" by N. Gopalswamy *et al.*, *J. Geophys. Res.*, *104*, 4743–4748.
- Cliver, E. W., D. F. Webb, and R. A. Howard (1999), On the origin of solar metric type II bursts, *Solar Phys.*, *187*, 89–114.
- Delaboudiniere, O., *et al.* (1995), EIT: Extreme-Ultraviolet Imaging Telescope for the SOHO mission, *Solar Phys.*, *162*, 291–312.
- Dryer, M. (1996), Comments on the origins of coronal mass ejections, *Solar Phys.*, *169*, 421–429.
- Dryer, M., S. T. Wu, R. S. Steinolfson, and R. M. Wilson (1979), Magnetohydrodynamic models of coronal transients in the meridional plane. II. Simulation of the coronal transient of 1973 August 21, *Astrophys. J.*, *227*, 1059–1071.
- Elmore, D. F., J. T. Burkepile, J. A. Darnell, A. R. Lecinski, and A. L. Stanger (2003), Calibration of a ground-based solar coronal polarimeter, *Proc. SPIE*, *4843*, 66–75.
- Fry, C. D., M. Dryer, Z. Smith, W. Sun, C. S. Deehr, and S.-I. Akasofu (2003), Forecasting solar wind structures and shock arrival times using an ensemble of models, *J. Geophys. Res.*, *108*(A2), 1070, doi:10.1029/2002JA009474.
- Gallagher, P. T., G. R. Lawrence, and B. R. Dennis (2003), Rapid acceleration of a coronal mass ejection in the low corona and implications for propagation, *Astrophys. J.*, *558*, L53–L56.
- Gergely, T. (1984), On the relative velocity of coronal transients and type II bursts, in *STIP Symposium on Solar/Interplanetary Intervals*, edited by M. A. Shea, D. F. Smart, and S. M. P. McKenna-Lawlor, p. 347, Bookcrafters, Chelsea, Mich.
- Gopalswamy, N. (2000), Type II radio bursts, in *Radio Astronomy at Long Wavelengths*, *Geophys. Monogr. Ser.*, vol. 119, edited by R. G. Stone *et al.*, p. 123, AGU, Washington, D. C.
- Gopalswamy, N., and M. R. Kundu (1992), Estimation of the mass of a coronal mass ejection from radio observations, *Astrophys. J.*, *390*, L37–L39.
- Gopalswamy, N., and M. R. Kundu (1993), Thermal and nonthermal emissions during a coronal mass ejection, *Solar Phys.*, *143*, 327–343.
- Gopalswamy, N., and M. R. Kundu (1995), Coronal shocks, interplanetary shocks and coronal mass ejections, in *Proceedings of the 2nd SOLTIP Symposium*, edited by T. Watababe, p. 177, Ibaraki Univ., Ibaraki, Japan.
- Gopalswamy, N., M. L. Kaiser, R. P. Lepping, S. W. Kahler, K. Ogilvie, D. Berdichevsky, T. Kondo, T. Isobe, and M. Akioka (1998), Origin of coronal and interplanetary shocks: A new look with Wind spacecraft data, *J. Geophys. Res.*, *103*, 307–316.
- Gopalswamy, N., M. L. Kaiser, R. P. Lepping, D. Berdichevsky, K. Ogilvie, S. W. Kahler, T. Kondo, T. Isobe, and M. Akioka (1999), Reply, *J. Geophys. Res.*, *104*, 4749–4754.
- Gopalswamy, N., A. Lara, M. L. Kaiser, and J.-L. Bougeret (2001), Near-Sun and near-Earth manifestations of solar eruptions, *J. Geophys. Res.*, *106*, 25,261–25,277.
- Gosling, J. T. (1993), The solar flare myth, *J. Geophys. Res.*, *98*, 18,937–18,950.
- Gosling, J. T., and A. J. Hundhausen (1995), Reply, *Solar Phys.*, *160*, 57–60.
- Guhathakurta, M., and R. Fisher (1998), Solar wind consequences of a coronal hole density profile: SPARTAN 201-03 coronagraph and ULYSSES observations from 1.15 R_{sun} to 4 AU, *Astrophys. J.*, *499*, L215.
- Harrison, R. A. (1986), Solar coronal mass ejections and flares, *Astron. Astrophys.*, *162*, 283–291.
- Harrison, R. A. (1995), The nature of solar flares associated with coronal mass ejection, *Astron. Astrophys.*, *162*, 304, 585.
- Harvey, K. L., S. F. Martin, and A. C. Riddle (1974), Correlation of a flare-wave and type II burst, *Solar Phys.*, *36*, 151.
- Howard, R. A., *et al.* (1997), Observations of CMEs from SOHO/LASCO, in *Coronal Mass Ejections*, *Geophys. Monogr. Ser.*, vol. 99, edited by N. Crooker, J. A. Joselyn, and J. Feynman, p. 17, AGU, Washington, D. C.
- Kahler, S., N. R. Sheely Jr., R. A. Howard, D. J. Michels, and M. J. Koomen (1984), Characteristics of flares producing metric type II bursts and coronal mass ejections, *Solar Phys.*, *93*, 133–141.
- Klassen, H. T., and H. Aurass (2002), On the association between type II radio bursts and CMEs, *Astron. Astrophys.*, *384*, 1098–1106.
- Kruger, A. (1979), *Introduction to Solar Radioastronomy and Radio Physics*, Springer, New York.
- Lara, A., N. Gopalswamy, S. Nunes, G. Munoz, and S. Yashiro (2003), A statistical study of CMEs associated with metric type II bursts, *Geophys. Res. Lett.*, *30*(12), 8016, doi:10.1029/2002GL016481.
- Leblanc, Y., G. A. Dulk, A. Vourlidas, and J.-L. Bougeret (2001), Tracing shock waves from the corona to 1 AU: Type II radio emission and relationship with CMEs, *J. Geophys. Res.*, *106*, 25,301–25,312.
- MacQueen, R. M., and R. R. Fisher (1983), The kinematics of solar inner coronal transients, *Solar Phys.*, *89*, 89–102.
- Mann, G., H. Aurass, A. Klassen, C. Estel, and B. J. Thompson (1999), Coronal transient waves and coronal shock waves, in *Proceedings of 8th SOHO Workshop*, *ESA SP-446*, pp. 447–481, Eur. Space Agency, Paris.
- Moon, Y.-J., G. S. Choe, H. Wang, Y.-D. Park, N. Gopalswamy, G. Yang, and S. Yashiro (2002), A statistical study of two classes of coronal mass ejections, *Astrophys. J.*, *581*, 694–702.
- Neupert, W. M., B. J. Thompson, J. B. Gurman, and S. P. Plunkett (2001), Eruption and acceleration of flare-associated coronal mass ejection loops in the low corona, *J. Geophys. Res.*, *106*, 25,215–25,226.

- Newkirk, G., Jr. (1961), The solar corona in active regions and the thermal origin of the slowly varying component of solar radio radiation, *Astrophys. J.*, *133*, 983.
- Parenti, S., B. J. I. Bromage, G. Poletto, G. Noci, J. C. Raymond, and G. E. Bromage (2000), Characteristics of solar coronal streamers. Element abundance, temperature and density from coordinated CDS and UVCS SOHO observations, *Astron. Astrophys.*, *363*, 800–814.
- Pick, M., et al. (1998), Joint Nancay radioheliograph and LASCO observations of coronal mass ejections: II. The 9 July 1996 event, *Solar Phys.*, *181*, 455–468.
- Robinson, R. D., and R. T. Stewart (1985), A positional comparison between coronal mass ejection events and solar type II bursts, *Solar Phys.*, *97*, 145–157.
- Reiner, M. J., M. L. Kaiser, N. Gopalswamy, H. Aurass, G. Mann, A. Vourlidas, and M. Maksimovic (2001), Statistical analysis of coronal shock dynamics implied by radio and white-light observations, *J. Geophys. Res.*, *106*, 25,279–25,290.
- Sakai, J. I., and C. de Jager (1996), Solar flares and collisions between current-carrying loops types and mechanisms of solar flares and coronal loop heating, *Space Sci. Rev.*, *1*, 1–192.
- Sawyer, C. S. (1985), Visibility and rate of coronal mass ejections, *Solar Phys.*, *98*, 369–378.
- Shanmugaraju, A., Y.-J. Moon, M. Dryer, and S. Umapathy (2003a), An investigation of solar maximum metric type II radio bursts: Do two kinds of coronal shock sources exist?, *Solar Phys.*, *215*, 164–184.
- Shanmugaraju, A., Y.-J. Moon, M. Dryer, and S. Umapathy (2003b), On the kinematic evolution of flare-associated CMEs, *Solar Phys.*, *215*, 185–201.
- Shanmugaraju, A., Y.-J. Moon, M. Dryer, and S. Umapathy (2003c), Statistical characteristics of CMEs and flares associated with solar type II radio bursts, *Solar Phys.*, *217*, 301–317.
- Sheeley, N. R., Jr., W. N. Hakala, and Y.-M. Wang (2000), Detection of coronal mass ejection associated shock waves in the outer corona, *J. Geophys. Res.*, *105*, 5081–5092.
- Svestka, Z. (1995), On “The solar flare myth” postulated by Gosling, *Solar Phys.*, *160*, 53–56.
- Vourlidas, A., S. T. Wu, A. H. Wang, P. Subramanian, and R. A. Howard (2003), Direct detection of a coronal mass ejection-associated shock in large angle and spectrometric coronagraph experiment white-light images, *Astrophys. J.*, *598*, 1392–1402.
- Vrsnak, B., V. Ruzdjak, P. Zlobec, and H. Aurass (1995), Ignition of MHD shocks associated with solar flares, *Solar Phys.*, *158*, 331–351.
- Webb, D. F., and R. A. Howard (1994), The solar cycle variation of coronal mass ejections and the solar wind mass flux, *J. Geophys. Res.*, *99*, 4201–4220.
- Willson, R. F., S. L. Redfield, K. R. Lang, B. J. Thompson, and O. C. St. Cyr (1998), First VLA observations of nonthermal metric bursts associated with coronal mass ejections detected by the solar and heliospheric observatory, *Astron. Astrophys.*, *504*, L117.
- Zhang, J., K. P. Dere, R. A. Howard, M. R. Kundu, and S. M. White (2001), On the temporal relationship between coronal mass ejections and flares, *Astrophys. J.*, *559*, 452–462.
- Zhang, M., L. Golub, E. Deluca, and J. Berkepille (2002), The timing of flares associated with the two dynamical types of solar coronal mass ejections, *Astrophys. J.*, *574*, L97–L100.

S.-C. Bong, K.-S. Cho, Y.-H. Kim, Y.-J. Moon, and Y.-D. Park, Korea Astronomy and Space Science Institute, Daejeon 305-348, Republic of Korea. (scbong@kasi.re.kr; kscho@kasi.re.kr; yhkim@kasi.re.kr; yjmoon@kasi.re.kr; ydperk@kasi.re.kr)

M. Dryer, NOAA Space Environment Center, Boulder, CO 80305, USA. (murray.dryer@noaa.gov)

C. D. Fry, Exploration Physics International, Inc., 6275 University Drive, Suite 37-105, Huntsville, AL 35806-1776, USA. (gfry@expi.com)

A. Shanmugaraju, Department of Physics, Arul Anandar College, Krumathur, 625 514, Madurai (Dt.), India. (shanmugaraju@yahoo.com)